LASE Measurements of Water Vapor, Aerosol, and Cloud Distributions in Saharan Air Layers and Tropical Disturbances

SYED ISMAIL[1], RICHARD A. FERRARE[1], EDWARD V. BROWELL[1,], SUSAN A. KOOI[2], JASON P. DUNION[3], GERRY HEYMSFIELD[4], ANTHONY NOTARI[2], CAROLYN F. BUTLER[2], SHARON BURTON[2], MARTA FENN[2], T. N. KRISHNAMURTI[5], GAO CHEN[1], AND BRUCE ANDERSON[1]

[1]*NASA Langley Research Center, Hampton VA 23681, USA;*
[2]*SSAI, Hampton, VA 23666, USA*
[3]*NOAA/AOML/Hurricane Research Division, Miami, FL 33149, USA*
[4]*NASA Goddard Space Flight Center, College Park, MD, USA*
[6]*University of Southern Florida, Tallahassee, FL 32306, USA*

Corresponding Author:

Syed Ismail, MS 401A, NASA Langley Research Center, Hampton VA 23681
e-mail: Syed.Ismail-1@nasa.gov; Phone:1-757-864-2719; Fax:1-757-864-7790

ABSTRACT

LASE (Lidar Atmospheric Sensing Experiment) on-board the NASA DC-8 measured high resolution profiles of water vapor and aerosols, and cloud distributions in 14 flights over the eastern North Atlantic during the NAMMA (NASA African Monsoon Multidisciplinary Analyses) field experiment. These measurements were used to study African easterly waves (AEWs), tropical cyclones (TCs), and the Saharan Air Layer(s) (SAL). Interactions between the SAL and tropical air were observed during the early stages of the TC development. These LASE measurements represent the first simultaneous water vapor and aerosol lidar measurements to study the SAL and its impact on AEWs and TCs. Examples of profile measurements of aerosol scattering ratios, aerosol extinction coefficients, aerosol optical thickness, water vapor mixing ratios, RH, and temperature are presented to illustrate their characteristics in SAL, convection, and clear air regions. LASE data suggest that the SAL suppresses low-altitude convection at the convection-SAL interface region. Mid-level convection associated with the AEW and transport are likely responsible for high water vapor content observed in the southern regions of the SAL on August 20, 2008. This interaction is responsible for the transfer of about 7×10^{15} J latent heat energy within a day to the SAL. Measurements of lidar extinction-to-backscatter ratios in the range 36 ± 5 to 45 ± 5 are within the range of measurements from other lidar measurements of dust. LASE aerosol extinction and water vapor profiles are validated by comparison with onboard *in situ* aerosol measurements and GPS dropsonde water vapor soundings, respectively.

1. Introduction

The NASA aircraft (NASA DC-8) component of the NAMMA (African Monsoon Multidisciplinary Analyses) field experiment was conducted from Sal Island, Cape Verde from 15 August to 12 September 2006 (Zipser et al., 2009). The main objectives of the NAMMA mission were to examine: 1) the formation and evolution of tropical cyclones (TCs) in the eastern and central North Atlantic that can eventually impact the U.S. east coast, 2) the composition and structure of the Saharan Air Layer (SAL), and 3) how aerosols affect cloud precipitation and influence TC development. The NAMMA campaign extended and complimented the international African Monsoon Multidisciplinary Analysis (AMMA) field experiment (Heywood et al., 2008). Because the SAL originates over continental Africa and propagates westward over the Atlantic Ocean, Cape Verde was chosen as the base of operations for the NASA DC-8. This aircraft carried an extensive payload of both remote and in situ instruments to characterize African Easterly Waves (AEWs) and the SAL and investigate their interactions in the region off the northwest coast of Africa, between the mainland and the eastern range limit of NOAA's research aircraft that were coordinating NAMMA research missions from Barbados (Zipser et al., 2009). The interaction of AEWs with the SAL and the potential development of AEWs into major Atlantic hurricanes is of great interest because nearly 85% of the intense (or major) hurricanes have their origins as easterly waves (Landsea, 1993) and over 90% of major hurricanes that impact the eastern U.S. originate off the west coast of Africa (Pasch and Avila, 1992).

The DC-8 instrument suite included NASA Langley Research Center's Lidar Atmospheric Sensing Experiment (LASE), which provided high spatial-resolution, vertical profiles of water vapor, aerosol backscatter, and cloud distributions along the aircraft flight track. Real-time LASE data were used to direct the DC-8 into regions of interest for *in situ* sampling during many flights. Dust layers associated with the SAL were embedded in large scale air masses that sometimes spanned 5000 km in horizontal extent and propagated westward from the African coast at regular intervals of 3-5 days. Zipser et al., (2009) and references therein summarize the state of interest and the need for fully understanding the nature and extent of influence of the SAL on the development of AEWs. LASE's simultaneous measurements of water vapor and aerosols provide a unique data set for characterizing SAL and AEW events and assessing the interactions between these two important meteorological features.

From analyses of satellite imagery and rawinsondes, Dunion and Velden (2004) have reported the large-scale structural and dynamical characteristics of the SAL. The SAL contains warm and dry air with a temperature inversion at the base (~800-900 hPa) and is associated with a midlevel easterly jet. Dunion and Velden point out that these characteristics of SAL tend to inhibit convection. This inference is also supported by other studies. A study of TC activity over a 25 year period over the Atlantic indicated a strong anti-correlation between TC activity and SAL events (Evan et al. 2006). Lau and Kim (2007a, b) suggest that dust within the SAL reduces the level of solar radiation reaching the surface, which in turn causes a lowering of the sea surface temperature. They point out that an excess of Saharan dust in the 2006 pre-monsoon season, as compared to 2005, was mainly responsible for reducing sea surface temperature in North Atlantic, possibly contributing to the marked decrease in TC activity in 2006. On the other hand, Karyampudi and Carlson (1988) concluded that the SAL is important, if not

necessary, in the initial development of AEWs. Karyampudi and Pierce (2002) found that the SAL had a positive influence on the genesis of two Atlantic storms through enhancement of baroclinic instability. The SAL can also influence cloud microphysical properties and act as a source of cloud condensation nuclei (CCN) enhancing convective intensity (Khain et al., 2005; Jenkins et al. 2008). Recent studies (Jenkins, 2008a; Towhy et al., 2009) using data collected during NAMMA show that SAL dust particles can act as CCN, which in turn can influence cloud microphysics, latent heat release, vertical transport and convection development and precipitation.

Water vapor concentration fields are a key component needed for understanding precipitation, evaporation, and latent heat release processes in cloud systems. The lack of adequate and accurate moisture measurements with sufficient vertical and horizontal resolutions limits the ability of most numerical models to represent these processes. Krishnamurti et al. (1994) found that deficiencies in the modeling of moisture and diabatic processes are due in part to the lack of knowledge of the tropical humidity fields. Model forecasts are very sensitive to the surface layer moisture. Krishnamurti et al. (1989) showed that models, which incorporated an explicitly resolved surface layer were able to more accurately compute the strong moisture flux between the ocean and atmosphere resulting in more accurate prediction of the formation of hurricanes. Results from the NASA Convection And Moisture Experiment (CAMEX) missions demonstrated the positive impacts of accurate, high resolution measurements of water vapor obtained by LASE on forecasts of hurricane track and intensity (Kamineni et al., 2003; 2006). To investigate the potential impact of the SAL on North Atlantic climatologies, Dunion and Marron (2008) used Caribbean rawinsondes to re-examine the Jordan (1958) mean hurricane season tropical sounding. They found that during the hurricane season, the tropical Atlantic is dominated by multiple atmospheric events (e.g. dry SAL and moist tropical non-SAL) and that a single mean sounding like Jordan's does not adequately represent unique air masses. LASE NAMMA high-resolution measurements provided an opportunity to study the influence of moisture distributions in the eastern Atlantic region on tropical storm development and to examine the 3-dimensional structure of the air masses described by Dunnion and Marron (2008). The mission also provided an opportunity to compare LASE data with other remote and *in situ* measurements. Some LASE observations related to individual SAL events during NAMMA have already been reported in the literature (Jenkins 2008a,b; Towhy et al., 2009, Zipser et al, 2009).

In this paper we present an overview of the LASE water vapor, aerosol, and cloud observations made during NAMMA. First, we briefly describe the LASE system and its data products, then review DC-8 flight tracks that show the large area surveyed during NAMMA. Examples of LASE observations over SAL and AEW events are presented for an improved characterization of these events and the impact of their interactions. LASE measurements of aerosol extinction and water vapor distributions are compared with *in situ* observations from the DC-8. A summary of the latitudinal distribution of moisture and associated SAL aerosol backscattering profiles is also presented.

2. LASE system and measurements during NAMMA

a. LASE system

The LASE DIAL system was developed at the NASA Langley Research Center in 1995 (Browell et al., 1997) and has subsequently participated in 12 field experiments while deployed onboard the NASA ER-2, P-3, or DC-8 aircraft (see e.g., Browell et al., 2005). LASE was operated onboard the DC-8 during NAMMA. The transmitter consists of a double-pulsed Ti:sapphire laser that operates in the 815-nm absorption band of water vapor and is pumped by a frequency-doubled Nd:YAG laser. Total laser output pulse energy is about 90 mJ in each of the on- and off-line laser pulse pairs that are transmitted at 5 Hz. This energy is nominally split in a 7:3 ratio for transmission in nadir and zenith directions, respectively. The nadir detector system uses two silicon avalanche photo diodes and three digitizers to cover a signal dynamic range of 10^6. During NAMMA, LASE operated locked to a strong water vapor absorption line at 817.223 nm and electronically tuned to other spectral positions on the side of the absorption line. In this mode, LASE transmitted up to three (on- and off-line) wavelength pairs to capture the full dynamic range of water vapor distributions. This method of operation permitted profiling of water vapor from near the surface to the upper troposphere and aerosol and cloud profiles from near the surface to the lower stratosphere. LASE has demonstrated the ability to measure high resolution water vapor distributions over the 0.01 gkg^{-1} to >20 gkg^{-1} mixing ratio range with an accuracy of 10% or 0.01 gkg^{-1}, whichever is larger (Browell et al, 1997). Measurements during a number of other field experiments have shown that LASE water measurements in the tropospheric regions agree well with other remote and *in situ* measurements (Ferrare et al., 2004, Behrendt et al., 2007)

b. LASE data products

LASE provided two main data products: profiles of water vapor mixing ratios (gkg^{-1}) and aerosol scattering ratios (ratio of aerosol to molecular backscattering corrected for water vapor absorption and estimated aerosol extinction). These digital data are available from the NASA Earth Observing System Data and Information System (EOSDIS) Data Centers. Images of LASE water vapor mixing ratio and aerosol scattering profiles are also available at http://asd-www.larc.nasa.gov/lidar/. Relative humidity profiles were also produced as secondary data products from LASE derived mixing ratio profiles and dropsonde/radiosonde temperature profiles.

Retrievals of aerosol extinction and aerosol optical depth profiles are the subject of ongoing research and are generated on a case-by-case basis. To derive aerosol extinction profiles from the LASE data, an estimate of the 'lidar ratio' or the ratio of extinction-to-backscatter (S_a) is needed. As an example, LASE measurements above and below an elevated dust layer observed on 20 August 2006 were used to determine transmission through the layer. The estimated transmission was then used to derive a value of the aerosol optical depth of the layer, which was then used to calculate an average S_a for the layer of 36 +/- 5 sr at the LASE wavelength of 817 nm. Note that this value is somewhat smaller than the value inferred from the results of Liu et al., 2007. They used data from the Cloud-Aerosol Lidar with Orthogonal Polarization (CALIOP) on the Cloud-Aerosol Lidar and Infrared Pathfinder Satellite Observations (CALIPSO) satellite to derive lidar ratios at 532 and 1064 nm for Saharan dust observed over the Atlantic Ocean and the Gulf of Mexico during August 2006, within a few days of the LASE measurements. The lidar ratios derived from the CALIOP data at two locations over the Atlantic Ocean were 41 ± 4 sr (532 nm) and 55 ± 5 sr (1064 nm) and 41 ± 6 sr (532 nm) and 54 ± 13 sr (1064 nm); note that the observed values of S_a at 1064 nm were considerably larger than the S_a =30 value modeled for the CALIOP dust aerosol that is used in the CALIOP

aerosol extinction retrieval algorithms (Liu et al., 2005, Omar et al., 2006). The value of S_a =36 reported here for the LASE measurements is within the wide range (30 to 80 sr) of measured S_a values corresponding to dust (for a review see e.g., Liu et al., 2007). As an example, Vaughan (2004) used data from the spaceborne Lidar in Space Technology Experiment (LITE) to derive values of S_a =26 +/- 4.8 sr (532 nm) and S_a =35 +/- 18.4 sr (1064 nm) for elevated dust layers near the Saharan desert. The variability in the lidar ratio is likely due to variations in size, composition, and shape of the dust particles, and RH. We used the LASE-derived S_a value of 36 along with a lidar inversion technique (Fernald, 1984) to derive profiles of unattenuated aerosol backscatter and extinction profiles throughout the mission. Aerosol optical depths for SAL layers are then obtained by integration of aerosol extinction profiles.

The aerosol scattering ratio and extinction profiles have a vertical resolution of 60 m and horizontal resolution of 2.1 km, whereas the water vapor mixing ratio and RH profiles have a vertical resolution of 330 m and horizontal resolution of 42 km.

c. DC-8/LASE flight tracks during NAMMA

DC-8 flight tracks are presented in Fig. 1 and illustrate the geographic coverage and density of the airborne data set. From a base of operations at Sal, Cape Verde, flights were conducted between 15 August and 12 September over a study area extending from near the coast of Africa to about 35°W and from about 6 to 22°N. LASE operated during all flights, but was unable to acquire data during portions of flights when the aircraft was in clouds. Seven AEWs and associated SAL events were sampled during the mission.

3. Examples of aerosol and water vapor distributions during AEWs with SAL events

a. 19 August 2006

A large-amplitude AEW 1 (the AEW numbering system is taken from Zipser et al., 2009) emerged from the coast of North Africa on 11 August 2006. Meteosat-8 and microwave-derived total precipitable water (TPW) satellite imagery from the constellation of EDMSP satellites and AMSR-E on Aqua indicated that beginning on 14 August, two features were evident near the eastern edge of this AEW: a well developed mesoscale convective system (MCS) along the southern portion of the AEW and a large SAL outbreak a few degrees north of that MCS. As the MCS tracked to the northwest over the next few days, it moved into the SAL environment to its north and by 17 August most of its associated convection had all but vanished. This same SAL outbreak began to move rapidly to the west-southwest and by the early evening of 18 August, it had completely overspread the Cape Verde Islands. Early that same day, a vigorous MCS (likely the precursor to Tropical Storm Ernesto) moved off the African coast and was positioned along the southern edge of this large SAL outbreak. Meteosat-8 and TPW satellite imagery also indicated that this MCS was located on the western edge of a relatively small amplitude AEW (AEW 2) that began moving off the coast early on 19 August (Fig. 2). The main segment of the SAL had an oval shape and extended from 10°N to >25°N in latitude.

NASA's DC-8 sampled a large SAL outbreak and AEW 2 on 19 August when the disturbance was located south of the Cape Verde Islands (Fig. 2). The main objectives of this mission included sampling the AEW that eventually formed Hurricane Ernesto, sampling the large SAL outbreak to its north, and coordinating a portion of the DC-8 flight track with an "A-Train" satellite overpass (e.g., CALIPSO and CloudSAT). Low- to mid-level cloud-drift and mid- to upper-level water vapor winds from UW/CIMSS (not shown) indicated that the vorticity

center associated with the MCS that was sampled that day was located south-southwest of the Cape Verde Islands, a few degrees to the west of the AEW wave axis. During this period, analyses from UW-CIMSS indicated that the tropical disturbance (AEW 2) was under the influence of 10-25 kt of northeasterly vertical wind shear and was associated with a broad area of east-west oriented low-level (850-925 hPa) convergence (not shown). The early and late portions of the DC-8 mission extensively sampled the dry, dusty air associated with the SAL outbreak that had overspread the Cape Verde Islands. The southern legs of this mission sampled the moist environment associated with the ITCZ and AEW.

On August 19 the MCS ahead of AEW 2 was situated near 7° N latitude, 26° W longitude, and the SAL was located to the north of the disturbance. Fig. 3a,b,c. show a cross-section of LASE measurements during the south to north (left to right on figure) segment (c—d in Fig. 2) of the flight. During this transect, the aircraft sampled the cirrus at 12 km in the south and then descended for *in situ* sampling of the SAL in the north. Fig. 3a shows the distribution of aerosols and clouds. To preserve the observations of clouds, these data have not been corrected for aerosol attenuation. Black (high scattering) regions indicate the locations of clouds and white (blank) areas indicate regions where no data are available due to severe attenuation by clouds or regions close to the aircraft where lidar signals are saturated. The structure of aerosol scattering associated with SAL is seen at higher latitudes over the 1-6 km altitude region. A number of dropsondes were released during this flight. The location of dropsondes during the a—b segment of the flight are shown by 'arrow marks' in Fig. 3a.

Fig. 3b shows water vapor mixing ratio profiles during this segment of the flight. Convection associated with AEW 2 was located to the south and a SAL outbreak was situated to the north. The southern segment shows deep convection (Fig. 3a) with high altitude cirrus (12 km). On the northern side of this convective region, there is an absence of high altitude clouds and very dry air (water vapor mixing ratios ~0.05 g/kg) appears to be subsiding to lower altitudes (near point A in Fig. 3b). This feature is fairly common in LASE data and is an indicator of subsidence that would accompany the deep convection to the south associated with the AEW 2 and the ITCZ. However, there are no direct observations of vertical winds in these very clean regions to confirm this. At the interface of the convection/SAL (at ~9°N), convection decreases as the aircraft begins overflying the SAL layer to the north suggesting that the SAL is associated with suppressed convection. The RH image (Fig. 3c) also shows generally low RH (35-55%) over most of the SAL region (indicated by high aerosol scattering regions up to 6 km in Fig. 3a).

Fig. 4 shows the temperature profile from the 18:13 UTC GPS dropsonde and a 1-minute average aerosol-scattering ratio profile from LASE. The temperature profile shows a strong inversion at the bottom of the SAL at ~800 m. At the top of this inversion at ~1.4 km a maximum in temperature of 24^0 C was observed. This maximum temperature was about 5.5^0 C higher at this altitude than the average (18.5^0 C) of all 82 GPS dropsondes launched in the region. There are changes in the lapse rate at 1.8, 3.5, 5.0, and 6.5 km altitudes that coincide with the aerosol (scattering) layers seen in the LASE images and Fig. 4. This illustrates the relationship between aerosol scattering and temperature structure in the SAL. Dropsonde temperature measurements within the SAL at other locations during this flight and on other flights show similar features. However, the higher temperatures at the base of the SAL, which was seen in many dropsonde observations, was not as high or as sharply peaked as that seen in Fig. 4. This is in contrast to other observations at the base of the SAL where the temperatures, in general, were 5-10° warmer than the Jordan (1958) mean hurricane season tropical sounding

(Diaz et al., 1976). Two factors could contribute to the lowering of the SAL temperature at its base: many of NAMMA flights were conducted in the vicinity of AEWs and the August/September temperatures may not be as high as those during more vigorous June and July outbreaks.

b. 20 August 2006

By 20 August, AEW 2 was located several hundred kilometers to the southwest of the Cape Verde Islands (Fig. 5). The day's airborne mission objectives included additional sampling of AEW 2 and the large SAL outbreak to its north, coordinating a portion of the DC-8 flight track with A-Train overpasses (e.g., CALIPSO and CloudSAT), and executing a microphysics profiling module in deep convection. This flight also provided a good opportunity to sample the transitional region between the AEW and the SAL and study their interactions. Analyses from UW-CIMSS indicated that AEW 2 remained under the influence of 10-25 kt of northeasterly vertical wind shear and was still associated with a broad area of east-west oriented, low-level (850-925 hPa) convergence (not shown).

By 20 August 2006 AEW 2 intensified and was interacting with the SAL outbreak to the north. The erosion in southern portions of the SAL in the neighborhood of the AEW can be seen from the satellite imagery (see the outline of the southern portions of the SAL in Fig. 5 compared to its outline in Fig. 2). LASE measurements from a segment (c—d in Fig. 5) of the flight are shown in Fig. 6. The general orientation of the flight during this segment was from the southwest to the northeast (left to right in Fig. 6). There is considerable convection in the southern tip of the SAL. Relative humidity profiles were derived from LASE water vapor mixing ratio and dropsonde/radiosonde temperature profiles that were interpolated to match the temporal resolution of LASE profiles. Clouds, with relative humidity values near 100%, are embedded and entrained within many sections of the SAL to the north. Cirrus clouds associated with deep convection reach high altitudes to the south and a cirrus shield covers the southern portions of the SAL to 15.6° N. High water vapor mixing ratios and high RH (70%) are observed over the whole segment of the SAL (Fig. 6b,c). This is in contrast to the example of the SAL in Fig. 3 with RH distributions in the range 35-60% (that are more characteristic of SAL events). High water vapor mixing ratios and high RH along with the mushroom shaped blooming of enhanced water vapor mixing ratios (and RH) on top of the mid-altitude cloud at locations A and B in Fig. 6 are indicators of convection as the source of enhanced moisture in this segment of the SAL. The presence of clouds and high moisture at B, C, and D are further indications of moistening of this lofted SAL by the interaction of the AEW through mid-altitude level convection

LASE data from a segment (segment a-b, highlighted red in Fig. 5) of the flight through AEW 2 to the south and the SAL to the north (left to right) are shown in the aerosol extinction profile image (Fig. 7). The lofted SAL is seen prominently in the altitude range 1-6 km in orange, green, and blue colors. Note that as the SAL emerges from the African coast it is undercut by a cool marine layer causing its base to gradually rise as it is advected further to the west. Low level convection in the southern region appears to decay at the SAL boundary (~12°N near 14:55 UTC), suggesting that some aspect of the dry, dusty continental air mass suppresses vertical transport. Aerosol optical thickness values obtained by integrating LASE-derived, aerosol extinction profiles over the altitude of the SAL (1.2 to 7 km) (black line plot in Fig 7a)

ranged from 0.05 to 0.4. A thin cirrus cloud layer is seen at 15:40 UTC at 7 km altitude. Attenuation of the lidar beam by clouds prevents retrievals of extinction profiles below the clouds (at point C). The aircraft flight conducted *in situ* sampling of the SAL from 15:40 to 16:40 UTC.

Water vapor mixing ratio and RH profiles related to the segment of flight in Fig. 7a are shown in Fig. 7b,c. High water vapor mixing ratios and high RH values (60-80%) are seen over much of the mid to upper regions of the SAL. Except for the presence of a thin cloud layer at 7 km near 15:40UTC, there is no direct evidence for this widespread moistening of the upper regions of SAL by direct convective processes. Moistening from upwind convection is apparently the source of the water vapor mixing ratios across this segment of the SAL (Fig. 7b). This moistening of the SAL is in contrast to the relatively low RH (35-55%) seen in SAL on the Aug. 19 flight (Fig. 3c).

Fig. 7a shows that low level convection has relatively insignificant influence on the SAL. Fig. 7c shows continuity in RH trail from low level convection in the lower left segment of the figure with higher RH in the SAL layer at point A. This is mainly due to the lower resolution of RH data compared to the aerosol scattering ratio (ASR) data shown in Fig. 7a. A close examination shows that the enhancements in aerosol scattering seen at point A and B are not well correlated with RH in Fig. 7c. However, there is significant enhancement of RH in the neighborhood (in the region near point D) of the cirrus (point C) indicating that the processes for development of the mid-level cirrus may be contributing to some enhancement of water vapor mixing ratios and RH in the SAL. The general enhancement of water vapor and RH in this SAL is probably the result of convection and transport from other locations. The SAL, in this case, is serving as a medium for storage of latent heat. It can also be seen that in some areas of the SAL the RH enhancements are correlated with higher aerosol scattering (E) and in other areas they are not. A portion of this non-correlation may be caused by variations in the hygroscopic properties of the aerosol particles due to their chemical composition, origin, and history (Twohey et al. 2009). Hygroscopic growth of dust in cloudy regions within the SAL was observed during one of the LASE flights during NAMMA (Twohey et al., 2009). It is likely that the SAL consists of some dust particles that are mildly hygroscopic from their origin or may have become hygroscopic later by interaction with atmospheric gases (Twohey et al., 2009). A study of the Gobi Desert dust particles mixed with pollution in Asian plumes indicated that the dust particles were not very hygroscopic (Howell et al., 2006).

Dunion and Velden (2004) argue that the SAL suppresses convection due to 1) the introduction of dry, stable air; 2) its mid-level easterly jet, which enhances vertical wind shear; and 3) the enhancement of the trade wind inversion. It is likely that the SAL, in general, tends to suppress convection. We postulate that interaction with the AEW is responsible for the rapid increase of about 2 gkg^{-1} water vapor over the altitude range 2-6 km in the SAL that occurred between19 August and 20 August 2006. A rough estimate of the transfer of the latent heat energy during this period was made by using LASE observations of the latitudinal extent of the SAL (~ 5^{o}), the shape of the SAL (Figs. 6 and 7), and longitudinal extent of the region of erosion of the SAL (~15^{o}, Fig. 5) containing enhanced water vapor. This net increase of the mass of water vapor in the SAL of about 2.9×10^{12} kg is equivalent to a transfer of energy of about 7×10^{15} J. This transfer of water vapor is equivalent to the transfer of about 65% of water vapor from AEW of about $5^{o}X5^{o}$ in size. Even smaller portions of such a rapid energy exchange (loss) could dampen the development of some weak AEWs. However, the SALs do not necessarily

appear to prohibit the development of stronger AEWs into major TCs, instead they act as a barrier/threshold for the development of AEWs.

Optical parameter measurements made by *in situ* sensors on the DC-8 during this portion of the flight provided an opportunity to assess the value of S_a and aerosol extinction profiles derived from the LASE data. Aerosol scattering and absorption coefficients measured with a three-wavelength TSI, Inc. nephelometer and a three wavelength Particle Soot Absorption Photometer (PSAP) (Chen et al., 2009, in this issue), respectively, were combined to derive aerosol extinction. Lidar signals measured below and above the SAL layer at this location were used to derive the aerosol optical depth and lidar ratio as described in Section 2b. The aerosol extinction profile obtained from LASE measurements at 16:32-16:33 UTC is compared with the *in situ* profiles in Fig. 8. The high LASE aerosol extinction values below ~700 m are due to the presence of low level boundary layer clouds. There is a very good agreement in magnitude and structure between the 450, 550 and 700 nm *in situ* and LASE 817 nm aerosol extinction profiles at this location. These data also illustrate the lack of wavelength-dependence in SAL extinction. DC-8 *in situ* size distribution measurements indicate the dust had a volume-mean diameter of between 2 and 3 mm, which yielded measured Angstrom Exponents of ≤ 0 (Chen et al., 2009, in this issue). Similar LASE-*in situ* comparisons performed on other days (9 August, 30 August, and 5 September, not shown) suggest that higher (40-45 sr at 817 nm) lidar ratios may produce even better agreement. This variation in the SAL lidar ratio is not surprising, since, as was discussed in Section 2b, S_a varies significantly with dust properties (i.e., size, shape, composition) and RH.

4. Moisture distributions and comparison with dropsondes

A vigorous AEW 4 emerged from the coast of North Africa early on 25 August 2006 behind a large SAL outbreak located to its north and west. This AEW emerged into the eastern North Atlantic at a fairly high latitude (~15-16°N) and tracked west-northwest over the next several days, moving directly into the nearby SAL. Not surprisingly, Meteosat-8 infrared satellite imagery indicated that the convection associated with this tropical disturbance rapidly dissipated as it tracked into the SAL's dry, dusty environment (Fig. 9). TPW imagery also indicated that as the AEW tracked over the eastern North Atlantic, the SAL outbreak out ahead of it began to wrap around the western and southern portions of the AEW's broad vorticity center.

NASA's DC-8 sampled the large SAL outbreak and the environment of the AEW on 26 August when the disturbance was located near the Cape Verde Islands (Fig. 9). The primary mission objectives were to map the AEW circulation, as well as the thermodynamics and aerosols of the surrounding SAL. Low-level cloud-drift winds and analyses from UW/CIMSS (not shown) indicated that the vorticity center associated with the AEW was located near ~15°N 28°W, just west-southwest of the Cape Verde Islands. Analyses from UW-CIMSS also indicated that during this period, the tropical disturbance (AEW) was under the influence of 5-20 kt of vertical wind shear and was associated with a broad area of low-level (850 hPa) vorticity. The DC-8 sampled the moisture associated with the AEW during the initial part of the mission (~1300-1500 UTC) and later sampled a SAL air mass that was wrapping around the southwest and southeast quadrants of the AEW circulation (~1500-1730 UTC). For most of the remainder

of the flight (~1730-2010 UTC), the aircraft sampled the moist environment associated with the AEW.

As shown in the water vapor distributions from the 26 August, 2006 flight (Fig. 10), convection was observed in the first half of the flight and near 1500 UTC. The DC-8 conducted *in situ* sampling of the air associated with the cirrus that was located at altitudes >6 km from 14:15 to 15:20 UTC. Water vapor measurements from LASE and the two sondes dropped into the high-moisture/cloudy and dry regions at points A and B (Fig. 10a), respectively, are compared in Figs. 10 b,c. Although the LASE profile is somewhat noisy due to cirrus-cloud attenuation, Fig. 10 b shows good agreement between the remote (LASE) and in situ (sonde) measurements. However, Fig. 10c shows excellent agreement between LASE and the dropsonde over the entire altitude range including the dry regions, which exhibited highly variable aerosol scattering. Trajectory analyses suggest that the very dry region (RH <10%) with low aerosol scattering ratio (<0.1) near 2 km altitude at 15: 40 UTC is a non-SAL air mass that may have been transported from the mid latitudes or descended from higher altitudes. Keil et al. (2008) have shown that low moisture at low altitudes suppresses convective development. The presence of low to mid-level dry air around the western and southern perimeter of the AEW on 26 August 2006 may be, in part, responsible for the non-development of this AEW. In addition, the presence of 5-20 kt of vertical wind shear and a broad area of low-level (850 hPa) vorticity may have also be contributing factors for the non development of the AEW.

A detailed comparison of LASE measurements with all dropsonde moisture profiles was performed for the NAMMA campaign. Mixing ratio profiles were derived from 82 dropsondes and compared with LASE (Fig. 11a,b). In general, LASE and dropsondes measurements agreed to within about 10 % over the full altitude range (Fig 11a). However, it was found that water vapor profiles measured by dropsondes that were manufactured in 2004 or earlier (model Rev. D/GPS1211) were consistently dryer than LASE water vapor profiles by 10% or more (Fig 11b). Water vapor profiles from dropsondes manufactured after 2004 (model Rev. F) were in much better agreement with the LASE water vapor profiles indicating that the older dropsondes had a dry bias.

5. Geographic distribution of water vapor and aerosols during NAMMA

a. Latitudinal distribution of aerosols and water vapor

As shown in Figure 12a, the latitudinal distribution of aerosol extinction profiles exhibits a broad region of enhanced extinction/aerosols below 6 km altitude (Fig. 12b,c) from about 7°N to areas well north of 21° N. A broad low-level peak in lower tropospheric aerosols was found near 17° N. The surface layer with high aerosol loading below 1 km altitude over the 12-22 ° N is thought to be the result of enhancement of mixed layer loading from the SAL on the boundary layer (Twohy et al., 2009; Chen et al., 2009). An enhancement in aerosols in the upper troposphere up to 15 km altitude associated with convective processes is seen at lower latitudes (< 10°N).. Low aerosol scattering (or aerosol extinction) thought to be associated with the general descending air at latitudes >17° N is seen in the altitude range 9-16 km. The overall average aerosol extinction profile for the whole campaign is given in Fig. 12b. No significant longitudinal dependence in SAL extinction was observed within the NAMMA study area (Figure 1). The average profile of the aerosol scattering ratio from all SAL events is shown in Figure 12c. Only events that met the criterion of aerosol scattering ratio exceeding 4.0 and a minimum layer thickness of 2 km were

used to denote SAL regions. Other observations are treated as non-SAL events. The aerosol optical depth of all SAL events ranged from 0.05 to 0.6 with an average of 0.3. The corresponding aerosol scattering ratios ranged up to 20 with an average of ~10 over the altitude region 2-6 km. In general, the altitude of SAL ranged from near the surface to about 6.5 km. Fig. 12d displays over 3900 LASE observations of cloud free atmospheric optical thickness (AOT) from surface (i.e., 30 m) to 8 km. These AOT values include an estimated seasalt AOT value of ~ 0.04 (Chen et al., 2009). Dust layers were observed in 2640 of the 3900 individual observations. The average SAL AOT is estimated at 0.36 ± 0.14. Using the mass extinction efficiency value of 0.8 m^2g^{-1} derived by Chen et al. (2009) from NAMMA *in situ* measurements, the average column dust mass loading is estimated to be 0.45 ± 0.14 g m^{-2}.

Latitudinal distributions of RH and water vapor mixing ratios are shown in Fig. 13a,b. RH values show a decrease in the range from about 11°N to 18°N over the 2-6-km altitude range associated with the presence of the SAL. RH and mixing ratio profiles over well defined SAL and non-SAL (events that did not meet the criterion of clear SAL events) regions are shown in Figs. 13c and d, respectively. For both parameters, SAL profiles are dryer than non-SAL events in the lower altitude region, but the differences above 3 km are not significant. This behavior is different from the observation of Dunion and Marron (2008), who show that in the 2002 hurricane season in the Caribbean, the SAL RH was lowest (~20%) near 500 mb compared to about 50% RH for non-SAL moisture at that altitude. Likewise, average NAMMA profiles indicate very little difference with the Dunion and Marron non-SAL moisture profiles. However, their SAL values are much dryer above 2 km, perhaps due to the NAMMA DC-8 sampling strategy that tended to specifically target AEWs. Note that the SAL dropsonde temperature profile (Fig. 13e) is slightly warmer than non-SAL profile near the base of the SAL. This explains the relatively lower RH in SAL regions compared to what is expected from the mixing ratio profiles. The average enhancement of temperature at the base of the SAL (near 2 km) was about 4° C compared to that in the non-SAL regions. The average SAL temperatures were warmer compared to temperature profiles from non-SAL region from the surface to 3 km and they were slightly cooler (~1° C) above 3 km.

6. Discussion and conclusions

LASE measurements from the NAMMA field experiment presented a unique opportunity to study the SAL in the vicinity of AEWs. From these LASE measurements the aerosol characteristics (profiles of aerosol scattering ratios, aerosol extinction coefficients, and aerosol optical depths) of the SAL and the water vapor distributions were derived. The characteristics of the SAL (high aerosol scattering, warm temperatures and inversions near the base, and vertical wind shear) are similar to those observed at other locations (Dunion and Velden, 2004). An analysis of Lase measurements in lofted SAL layers yielded aerosol extinction-to-backscatter ratios (lidar ratios) in the 36 to 45 +/- 5 sr range at the 817 nm wavelength; extinction profiles derived using these values agreed well with soundings calculated from in situ measurements. Temperature profiles from GPS dropsondes show the characteristic temperature inversion at the base of the SAL with significantly enhanced temperatures at the top of this inversion. The average temperature at the base of the SAL at about 2 km altitude was higher than the non-SAL (mixture) temperature by about 4°C. The average SAL temperature below about 3 km altitude was warmer than the moist tropical non-SAL environment, and above 3 km it was slightly lower (by ~1°C). SAL aerosol optical depths ranged from 0.05 to 0.6 and averaged 0.36 ± 0.14. The

aerosol scattering ratios in the middle of the SAL ranged from 10-20. The altitude of the top of the SAL ranged up to 6.5 km while the bottom of many of these layers merged with the marine boundary layer. Changes in lapse rate with altitude were found to coincide with layering of aerosols within the SAL. These LASE measurements can be coupled with retrievals of radiation fluxes at the top of the atmosphere (TOA), at the surface and within the atmosphere from the Clouds and Earth Radiant Energy System (CERES) instruments that operated during NAMMA aboard the Terra and Aqua spacecraft to study the impact of the SAL on the radiation budget throughout the atmospheric column. These studies would also improve our understanding of the thermodynamic environment in the region and address important questions regarding the effect of the SAL on atmospheric temperature structure and stability and regional sea-surface temperatures. Although some observations were made of the SAL away from convective regions, the objective of many of the DC-8 flights was to study the environment of AEWs and their interactions with SAL. Many examples from LASE suggest that the SAL suppresses low level convection seen at the interface of the SAL and the tropical convective regions. As discussed by Dunion and Velden (2004), the SAL is associated with stable dry air and wind shear that are likely to suppress convection. Our observations indicate that SAL-AEW interactions lead to the rapid transfer of latent heat energy (water vapor) to the SAL and the concomitant mixing of dust into the adjacent cloudy regions. The transfer of the water vapor to the SAL is likely from mid-level convection and transport. By comparison of water vapor measurements during 19-29 August 2006 and satellite imagery it was estimated that this interaction was responsible for the transfer of about 7×10^{15} J latent heat energy within a day to the SAL. This loss of latent heat energy is equivalent to that of about 65% of the water vapor contained within a small ($5^{o}X5^{o}$) AEW. This transfer of energy, in the absence of other mechanisms that intensify AEWs, could suppress development of weak AEWs. However, the SAL does not necessarily limit the eventual development of stronger AEWs into strong TCs as was observed in the development of many strong storms during NAMMA (TS Ernesto and Debby and Hurricane Helene).

Except for the regions that were totally obscured by lidar signal attenuation by clouds, LASE measurements of water vapor demonstrated the capability to capture the full dynamic range of water vapor distributions over the entire range of flights. Such measurements are known to improve water vapor data assimilation and numerical weather forecasts (Rizvi and Bensman, 2002, Wulfmeyer et al., 2006). Forecast studies at Florida State University are in progress that show a strong sensitivity to and improvements in forecasts to LASE water vapor profiles. The results of these will be reported in a separate publication (Krishnamurti et al., 2009) Water vapor mixing ratio profiles from NAMMA, in general (that were away from pristine SAL layers), were found to be similar to the tropical water vapor profile observed by Dunion and Marron (2008) in the Caribbean during the hurricane season. LASE measurements of a wide range of water vapor distributions during this mission were compared with *in situ* GPS dropsonde measurements and agreed well within 10%. However, dropsondes from an older batch (Rev. D/GPS1211 dropsondes) that were manufactured before 2004) were found to have a significant dry bias.

In a recent review of the NAMMA waves, Zipser et al (2009), elucidates many unsolved research areas where they express the strong sensitivity of tropical wave behavior to the prevailing dry and or wet conditions.
While referring to waves north or south of 15N they stated that" the northern systems were typically at low levels and dry while the southern systems typically were in mid-troposphere and rainy." These are the types of systems where a moisture analysis from LASE and its assimilation in mesoscale models can help in providing a clearer distiction among these northern and southern

systems. On the NOAA/AOML/Hurricane Research Division's first Saharan Air Layer Experiment (SALEX) they state that "The main objectives of SALEX include improving the understanding and prediction how the SAL's dry air, mid-level easterly jet, and suspended mineral dust affect Atlantic TC intensity change and assessing how well these components of the SAL are being represented in forecast models." These are again, clearly those areas where the LASE based analysis of the atmospheric state can help modeling and further understanding of the SALEX issues. On SAL they ask ," Are the most important influences of the SAL the ingestion of dry air into the wave " Such injections of dry air can be seen from the water vapor channel imagery from satellites, but for quantitative understanding via modeling we need a better four dimensional assimilation of moisture, here LASE can provide the vertical and horizontal details of these dry air intrusions. The operational models provide descriptions of moisture that carry large wet or dry biases. LASE measurements on 20 August 2009 already show the enhancement of moisture of the SAL from interactions with AEW 2. Further, they state "Additionally, profiles of RH from collocated GFS and GFDL model analysis suggest that although both models were capturing the general moisture trends below, within, and above the SAL, they tended to overestimate the SAL's mid-level dryness. For the small sample shown, GFS and GFDL overestimated the SAL's mid-level moisture by as much as 40-50% RH." Clearly having a mobile LASE observing system that can provide data in critical areas , the model reanalysis can provide very useful corrections from the deployment of LASE.

Acknowledgements: We thank: Paul McClung for supporting LASE integration onto the DC-8; Dr. Ramesh Kakar, NASA Headquarters, for providing financial support for LASE deployment and data analysis; Dr. Edward Zipser for coordinating and directing the NAMMA field experiment; and Dr. George Smith for discussions on the radiative effects of the SAL.

REFERENCES

Behrendt, A., V. Wulfmeyer, P. D. Gilarmo, C. Kimele, H-S. Bauer, T. Schaberl, D. Summa, D. N. Whiteman, B. B. Demoz, E. V. Browell, S. Ismail, R. Ferrare, S. A. Kooi, G. Ehret, and J. Wang, 2007: Intercomparison of water vapor data measured with lidar during IHOP_2002. Part I: airborne to ground-based lidar systems and comparison with Chilled-Mirror hygrometer radiosondes, 2007: *J. Atmos. Oceanic Technol.*, **24**, 3-21.

Browell, E. V.; Grant, W. B.; and Ismail, S.: Airborne Lidar Systems, in *Laser Remote Sensing*, edited by Takashi Fujii and Tetsuo Fukuchi, Taylor & Francis, NY, pp. 723-779, 2005.

Browell, E. V., S. Ismail, W. M. Hall et al., 1997: LASE Validation Experiment, in *Advan. in Atmos. Remote Sensing With Lidar*, A. Ansman, R. Neuber, P. Rairoux, and U. Wandinger (Eds.), Springer, pp 289-295.

Chen, G. et al. 2009. (In this issue)

Diaz, H. F.., T. N. Carlson, and J. M. Prospero, 1976: A study of the structure and dynamics of the Saharan air layer overt the northern equatorial Atlantic during BOMEX. National

Hurricane and Experimental Meteorology Laboratory NOAA Tech. Memo. ERL WMPO-32, 61 pp.

Dunion, J.P., and C.S. Velden, 2004: The impact of the Saharan Air Layer on Atlantic tropical cyclone activity. *Bull. Amer. Meteor. Soc.,* **85**, 353-365.

Dunion, J. P., and C. S. Marron, 2008: A reexamination of the Jordan mean tropical sounding based on awareness of the Saharan Air Layer: Results from 2002, *J. Climate*, **21**, DOI: 10.1175/2008JCLI1868.1.

Evan, A. T., J. Dunion, J. A. Foley, A. K. Heidinger, and C. S. Velden, 2006: New evidence for a relationship between Atlantic tropical cyclone activity and African dust outbreaks, *Geophys. Res. Lett.*, **33**, L19813, doi:10.1029/2006GL026408.

Ferrare, R., S. Ismail, E. Browell et al., 2000: Comparison of aerosol optical properties and water vapor among ground and airborne lidars and Sun photometers during TARFOX, *J. Geophys. Res.*, **105**, 9917-9933.

Ferrare, R.A., E.V. Browell, S. Ismail, S. Kooi, L.H. Brasseur, V.G. Brackett, M. Clayton, J. Barrick, H. Linné, A. Lammert, G. Diskin, J. Goldsmith, B. Lesht, J. Podolske, G. Sachse, F.J. Schmidlin, D. Turner, D. Whiteman, D. Tobin, H. Revercomb, 2004: Characterization of upper troposphere water vapor measurements during AFWEX using LASE, *J. Atmos. Oceanic Tech.,* **21**, 1790-1808.

Haywood, J. M., J. Pelon, P. Formenti, N. Bharmal, M. Brooks, et al., 2008: Overview of the Dust and Biomass-burning Experiment and African Monsoon Multidisciplinary Analysis Special Observing Period-0, *J. Geophys. Res.*, **113**, doi:10.1029/2008JD010077.

Howell, S. G., A. D. Clarke, Y. Kapustin, C. S. McNaughton, S. J. Doherty, and T. L. Anderson, 2006: Influence of relative humidity upon pollution and dust during ACE-Asia: size distributions and implications for optical prperties, *J. Geophys. Res.*,. **111,** D06205, doi:10.1029/2004JD005759, 2006.

Jenkins, G.S., A, Pratt, and A. Heymsfield, 2008: Possible linkages between Saharan dust and Tropical Cyclone Rain Band Invigoration in Eastern Atlantic during NAMMA-06. *Geophys. Res. Lett.,* **35,** L08815, doi:10.1029/2008GL034072.

Jenkins, G. S. and A. Pratt, 2008: Saharan Dust, Lightning and Tropical Cyclones in the Eastern Tropical Atlantic during NAMMA-06. *Geophys. Res. Lett.,* **35**, L12804, doi:10.1029/2008GL033979.

Kamineni, R., T. N. Krishnamurti, R. A. Ferrare, S. Ismail, and E. V. Browell, 2003: *Geophysical Research Letter*s, **30**, 1234.

Kamineni, R., T.N. Krishnamurti, S.Pattnaik , E. V. Browell, S. Ismail, R. A. Ferrare, 2006: Impact of CAMEX-4 Data Sets for Hurricane Forecasts using a Global Model, *J. Atmos. Sci.* **63**, 151-174.

Karyampudi, V.M. and T.N. Carlson, 1988: Analysis and numerical simulations of the Saharan air layer and its effect on easterly wave disturbances. *J. Atmos. Sci.*, **45**, 3102-3136.

Karyampudi, V.M. and H.F.Pierce, 2002: Synoptic-scale influence of the Saharan air layer on tropical cyclogenesis over the eastern Atlantic. *Mon. Wea.Rev.*, **130**, 3100-3128.

Keil, C., A. Röpnack, G. C. Craig, and U. Schumann, 2008: Sensitivity of quantitative precipitation forecast to height dependent changes in humidity, *Geophys. Res. Lett.*, **35**, L09812, doi:10.1029/2008GL033657.

Khain, A., D. Rosenfeld, and A. Pokrovsky, 2005: Aerosol impact on the dynamics and microphysics of deep convective clouds. *Q. J. R. Meteorol. Soc.,* **131**, 2639-2663.

Krishnamurti, T. N. and D. Oosterhof, 1989: Prediction of the life cycle of a supertyphoon with a high resolution global model. *Bull. Am. Meteor. Soc,.***70**, 1218.

Krishnamurti, T. N., with G. Rohaly and H. S. Bedi, 1994: On the improvement of precipitation forecast skill from physical initialization. *Tellus.* **46A**, 598-614.

Landsea, C.W. (1993): "A climatology of intense (or major) Atlantic hurricanes" Mon. Wea. Rev., 121, pp.1703-1713.

Lau, K. M., and K. M. Kim, 2007a: Cooling of the Atlantic by Saharan dust, *Geophy. Res. Lett.*,34, L23811, doi:10.1029/2007GL031538.

Lau, K. M., and K. M. Kim, 2007b: How nature foiled the 2006 hurricane forecasts, *Eos Trans. AGU*, **88**(9), 105.

Liu, Z., A. Omar, Y. Hu, M. Vaughan, and D. Winker , 2005:, CALIOP Algorithm Theoretical Basis Document—Part 3: Scene classification algorithms, Release 1.0, PC-SCI-202, NASA Langley Res. Cent., Hampton, Va. (Available at http://www-calipso.larc.nasa.gov/resources/project_documentation.php)

Liu, Z., et al. 2008: CALIPSO lidar observations of the optical properties of Saharan dust: A case study of long-range transport, J. Geophys. Res., **113**, D07207, doi:10.1029/2007JD008878.

Omar, A., D. Winker, J. Won, and M. Vaughan 2006: Selection algorithm for the CALIPSO lidar aerosol extinction-to-backscatter ratio, in Reviewed and Revised Papers Presented at the 23rd International Laser Radar Conference, edited by C. Nagasawa and N. Sugimoto, pp. 937–940, Tokyo Metropolitan Univ., Tokyo.

Rizvi, S. R. H., E. L. Bensman, T. S. V. Vijay Kumar, A. Chakrborty, and TN Krishnamurti, 2002: Impact of CAMEX-3 data on the analysis and forecasts of Atlantic Hurricanes, *Meteo. Atmos. Phys.*, **79**, 13-32.

Twohy, C. H., Kreidenweis, T. Eidhammer, E. V. Browell, A. J. Heymsfield, A.R. Bansemer, B. E. Anderson, G. Chen, S. Ismail, P. J. DeMott and S. Van den Heever, 2008: Saharan dust particles nucleate droplets in eastern Atlantic clouds. Geophys. Res. Lett., 36, L01807, doi:10.1029/2008GL035846.

Vaughan, M. (2004), Algorithm for retrieving lidar ratios at 1064 nm from space-based lidar backscatter data, *Proc. SPIE Int. Soc. Opt. Eng.*, **5240**, 104–115.

Wulfmeyer, V., H-S Bauer, M. Grezeschik, A, Behrendt, F. Vandenberghe, E. V. Browell, S. Ismail, and R. A. Ferrare, 2006: 4-dimentional variational assimilation of water vapor differential absorption lidar data: The first case study within IHOP 2002, *Mon. Wea. Rev.*, **134**, pp. 209–230.

Zipser, E. J., C. H. Twohy, S.-C. Tsay, K. L. Thornhill, S. Tanelli, R. Ross, T.N. Krishnamurti, Q. Ji, G. Jenkins, S. Ismail, N. C. Hsu, R. Hood, G. M. Heymsfield, A. Heymsfield, J. Halverson,M. W. Goodman, R. A. Ferrare, J. P. Dunion, M. Douglas, R. Cifelli, G. Chen, E. V. Browell, B. Anderson, 2009: The Saharan air layer and the fate of African Easterly Waves, NASA's AMMA 2006 Field Program to Study Tropical Cyclogenesis: NAMMA, (*in press*), *Bull. Amer. Meteor. Soc.*

Figure captions:

Fig. 1. Flight tracks of DC-8 during the NAMMA mission.

Fig. 2. METEOSAT-8 Split window image showing the distribution of the SAL on 19 Aug 2006. The DC-8 flight track is also shown and the segment of data shown in Fig. 3 is highlighted by red dash lines. The location of Sal Island, Cape Verde, Africa is indicated by the blue star symbol.

Fig. 3. LASE measurements of a) aerosol scattering ratio profiles; b) water vapor mixing ratio profiles; and c) RH profiles associated with the SAL event on 19 Aug. 2006. The locations of dropsondes release are indicated by arrow marks (Fig. 3a). Blank regions indicate data void regions due to cloud attenuation or in data blind regions close to the aircraft. The altitude of the aircraft is indicated by dotted line. Significant loss of data occurs during aircraft ascent , descent, and when the aircraft is at low altitudes.

Fig. 4. Dropsonde temperature measurements at 18:13 UTC compared with LASE measurements of aerosol scattering ratios associated with the SAL event on 19 Aug. 2006.

Fig. 5. METEOSAT-8 Split window image showing the distribution of the SAL on 20 Aug 2006. The DC-8 flight track is also shown and the segments of data shown in Fig. 6 and Fig. 8 are highlighted by red dash lines and black dash respectively. The location of Sal Island, Cape Verde, Africa is indicated by the blue star symbol.

Fig. 6. LASE measurements a) aerosol scattering ratio profiles; b) water vapor mixing ratio; and c) RH profiles from the c--d segment of flight on 20 Aug. 2006 (Fig. 5).

Fig. 7. LASE measurements a) aerosol extinction profiles; b) water vapor mixing ratio; and c) RH profiles from the a---b segment of flight on 20 Aug. 2006 (Fig. 5). The profile of aerosol optical depth (black line) of the SAL is overlaid on the aerosol extinction image (Fig. 7a).

Fig. 8. Aerosol extinction profiles from LASE compared with *in situ* measurements from LARGE. The high scattering at 0.5 km seen in the LASE data are from a low altitude cloud.

Fig. 9. METEOSAT-8 Split window image showing the distribution of the SAL on 26 Aug 2006. The DC-8 flight track is also shown and the segment of data shown in Fig. 10 is highlighted by red dash lines. The location of Sal Island, Cape Verde, Africa is indicated by the star symbol.

Fig. 10. a) LASE measurements of water vapor mixing ratio distribution on 26 Aug. 2006 associated with an AEW and the surrounding dry air region, comparison of LASE water vapor mixing ratio with GPS dropsonde measurements identified at location; b) A in Fig. 10a; and c) B in Fig. 10a.

Fig. 11. Comparison of LASE water vapor mixing ratio measurements a) new dropsondes and b) old dropsondes that were manufactured before 2001. The red error bars indicate the standard deviation of the differences and the green bars indicate the standard error.

Fig. 12. a) Latitudinal distribution of aerosol extinction profiles measured by LASE during NAMMA; b) average aerosol extinction profile from all observations; c) average aerosol scattering ratio profile from clearly identified SAL regions.

Fig. 13. a) Latitudinal distribution of RH distribution derived from LASE mixing ratio and dropsonde temperature profiles; b) latitudinal distribution of water vapor mixing ratios; c) average RH profile from all observations over the clearly identified SAL events and non-SAL (mixture) events; d) average water vapor mixing ratio profiles from SAL and non-SAL (mixture) events; and e) vertical profile of temperature from dropsondes from SAL and non-SAL events.

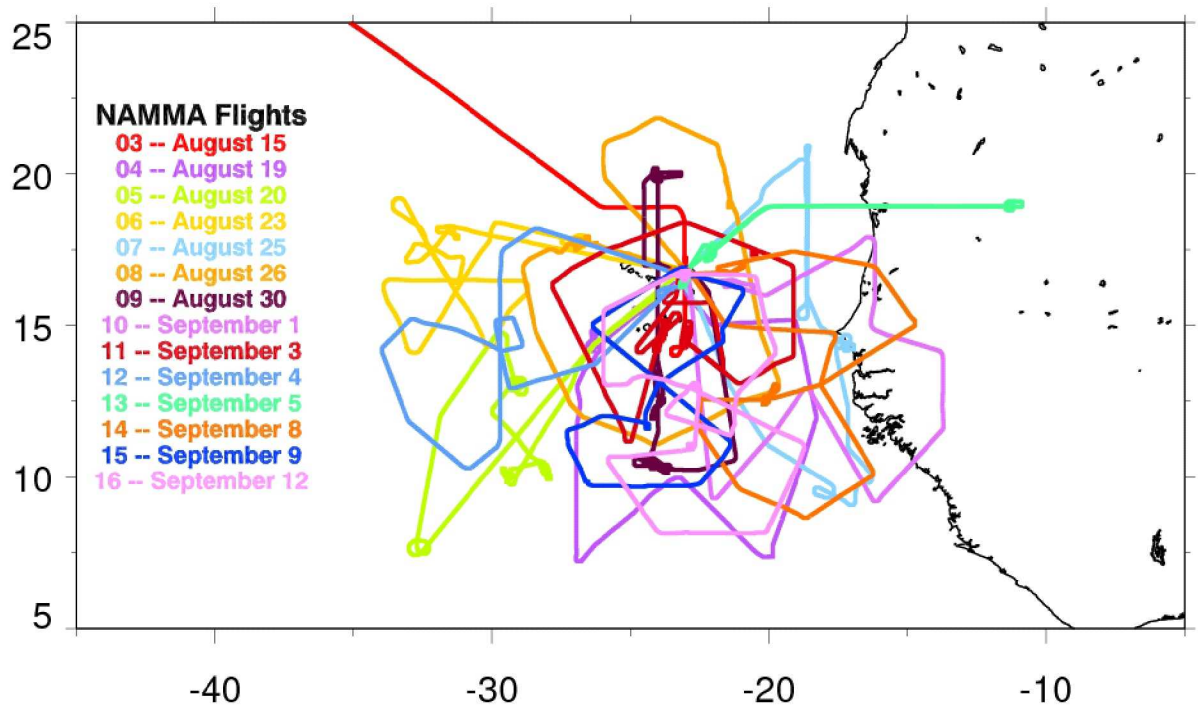

Fig. 1. Flight tracks of DC-8 during the NAMMA mission.

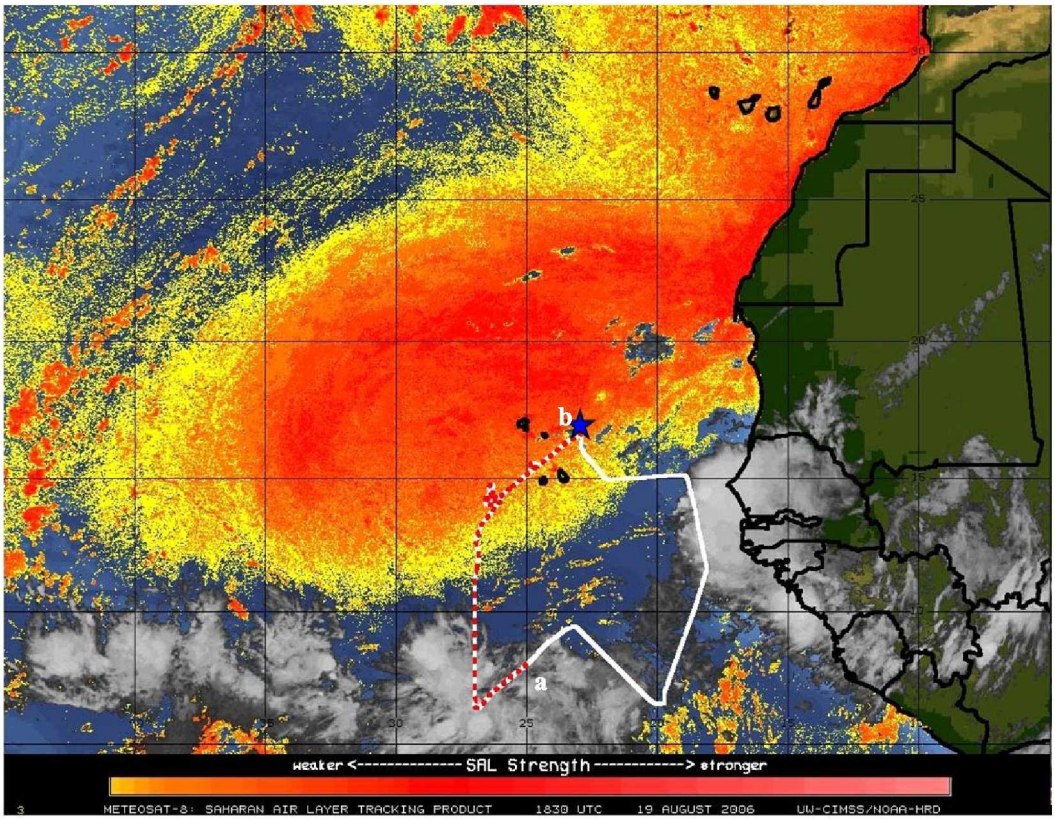

Fig. 2. METEOSAT-8 Split window image showing the distribution of the SAL on 19 Aug 2006. The DC-8 flight track is also shown and the segment of data shown in Fig. 3 is highlighted by red dash lines. The location of Sal Island, Cape Verde, Africa is indicated by the blue star symbol.

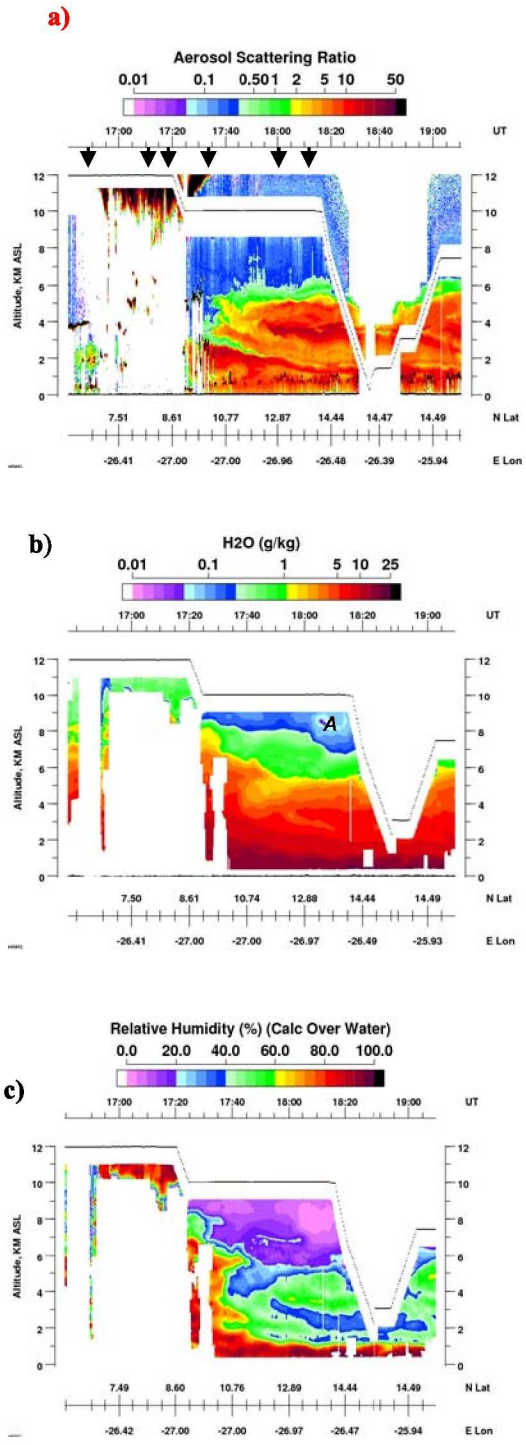

Fig. 3. LASE measurements of a) aerosol scattering ratio profiles, b) water vapor mixing ratio profiles, and c) RH profiles associated with the SAL event on 19 Aug. 2006. The locations of dropsondes release are indicated by arrow marks (Fig. 3a). Blank regions indicate data void regions due to cloud attenuation or in data blind regions close to the aircraft. The altitude of the aircraft is indicated by dotted line. Significant loss of data occurs during aircraft ascent and descent, and when the aircraft is at low altitudes.

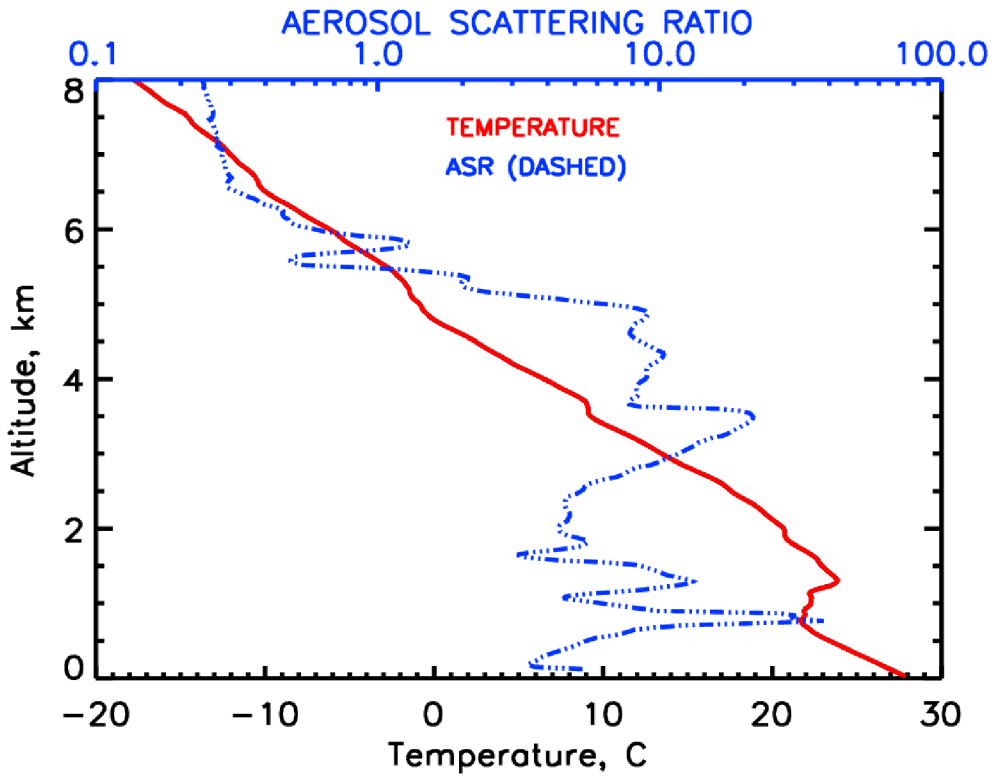

Fig. 4. Dropsonde temperature measurements at 18:13 UTC compared with LASE measurements of aerosol scattering ratios associated with the SAL event on 19 Aug. 2006.

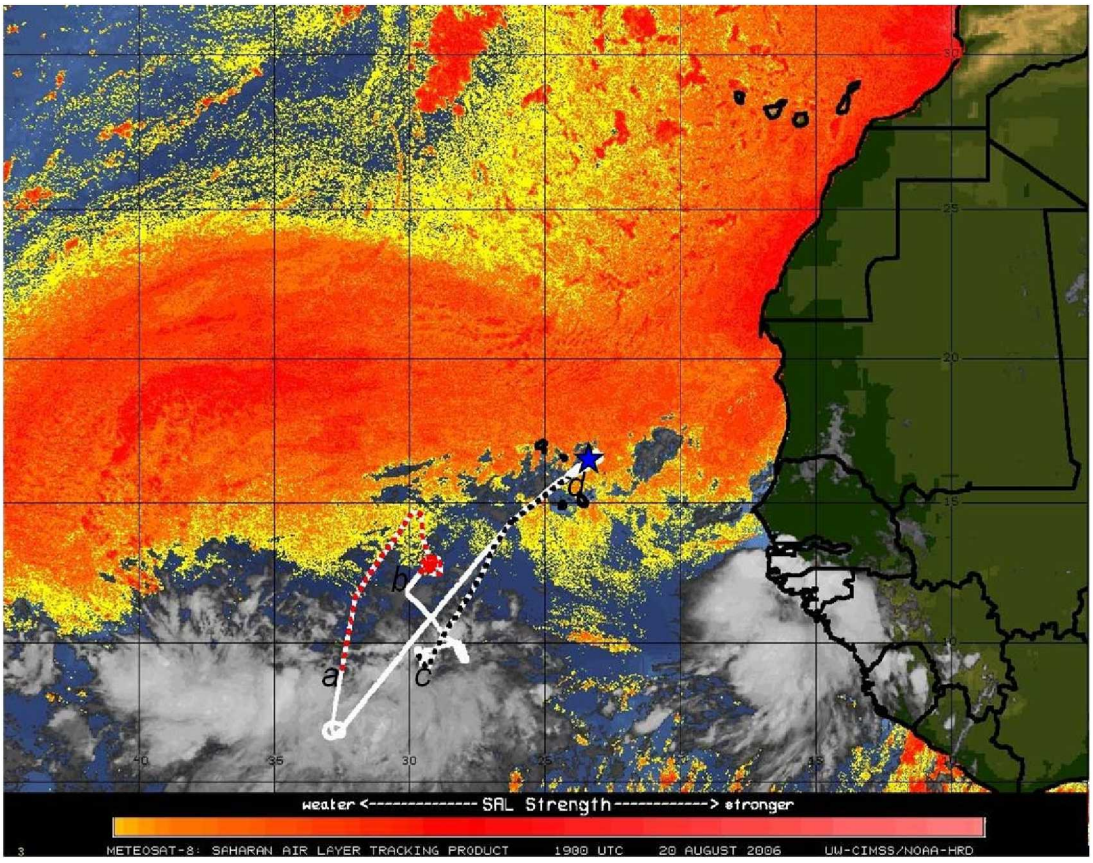

Fig. 5. METEOSAT-8 Split window image showing the distribution of the SAL on 20 Aug 2006. The DC-8 flight track is also shown and the segments of data shown in Fig. 6 and Fig. 8 are highlighted by red dash lines and black dash respectively. The location of Sal Island, Cape Verde, Africa is indicated by the blue star symbol.

a)

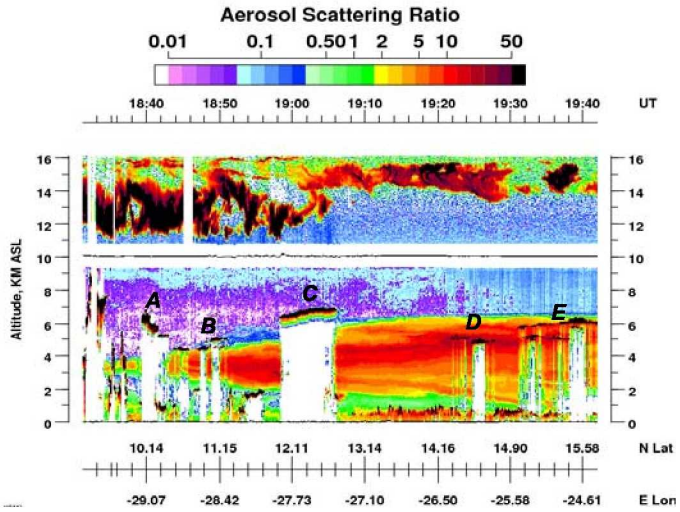
Aerosol Scattering Ratio
0.01 0.1 0.5 1 2 5 10 50
18:40 18:50 19:00 19:10 19:20 19:30 19:40 UT
Altitude, KM ASL
A
B
C
D
E
10.14 11.15 12.11 13.14 14.16 14.90 15.58 N Lat
-29.07 -28.42 -27.73 -27.10 -26.50 -25.58 -24.61 E Lon

b)

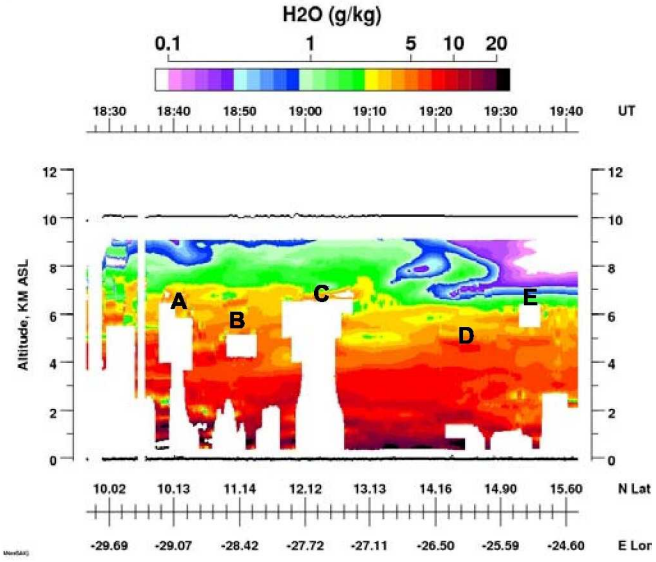
H2O (g/kg)
0.1 1 5 10 20
18:30 18:40 18:50 19:00 19:10 19:20 19:30 19:40 UT
Altitude, KM ASL
A
B
C
D
E
10.02 10.13 11.14 12.12 13.13 14.16 14.90 15.60 N Lat
-29.69 -29.07 -28.42 -27.72 -27.11 -26.50 -25.59 -24.60 E Lon

c)

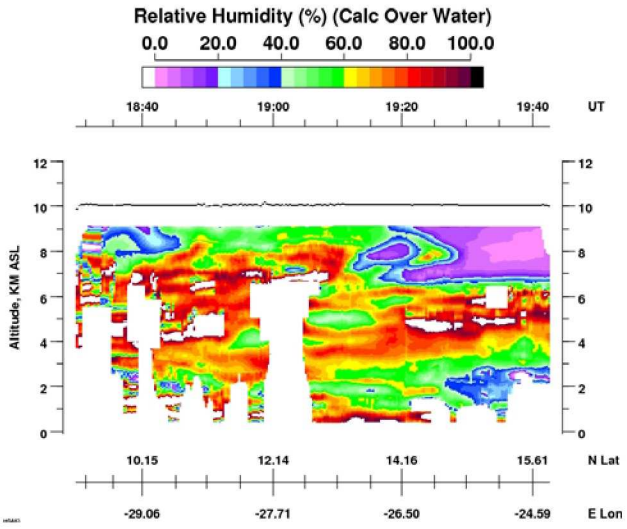

Fig.6. LASE measurements a) aerosol scattering ratio profiles, b) water vapor mixing ratio profiles, and c) RH profiles from the c--d segment of flight on 20 Aug. 2006 (Fig. 5). The profile of aerosol optical depth (black line) of the SAL is overlaid on the aerosol extinction image (Fig 6a).

a)

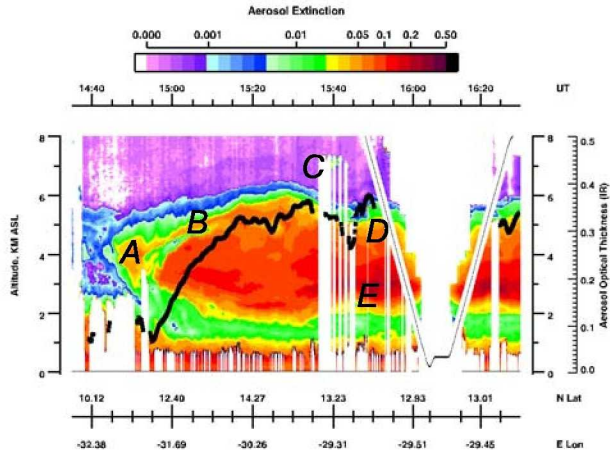
Aerosol Extinction
0.000 0.001 0.01 0.05 0.1 0.2 0.50
14:40 15:00 15:20 15:40 16:00 16:20 UT
Altitude, KM ASL
Aerosol Optical Thickness (IR)
A
B
C
D
E
10.12 12.40 14.27 13.23 12.93 13.01 N Lat
-32.38 -31.69 -30.26 -29.31 -29.51 -29.45 E Lon

b)

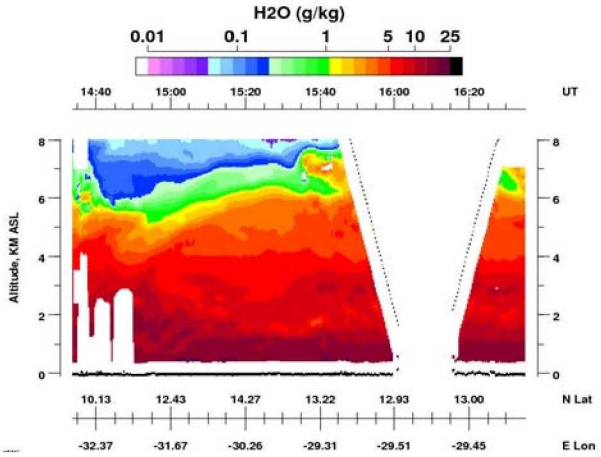
H2O (g/kg)
0.01 0.1 1 5 10 25
14:40 15:00 15:20 15:40 16:00 16:20 UT
Altitude, KM ASL
10.13 12.43 14.27 13.22 12.93 13.00 N Lat
-32.37 -31.67 -30.26 -29.31 -29.51 -29.45 E Lon

c)

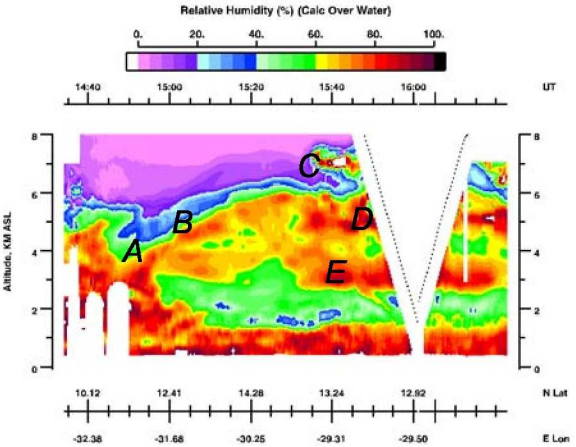
Relative Humidity (%) (Calc Over Water)
0. 20. 40. 60. 80. 100.
14:40 15:00 15:20 15:40 16:00 UT
Altitude, KM ASL
A
B
C
D
E
10.12 12.41 14.28 13.24 12.92 N Lat
-32.38 -31.68 -30.25 -29.31 -29.50 E Lon

Fig. 7. LASE measurements a) aerosol extinction profiles and b) water vapor mixing ratio profiles, and c) RH profiles from the a---b segment of flight on 20 Aug. 2006 (Fig. 5). The profile of aerosol optical depth (black line) of the SAL is overlaid on the aerosol extinction image (Fig. 6a).

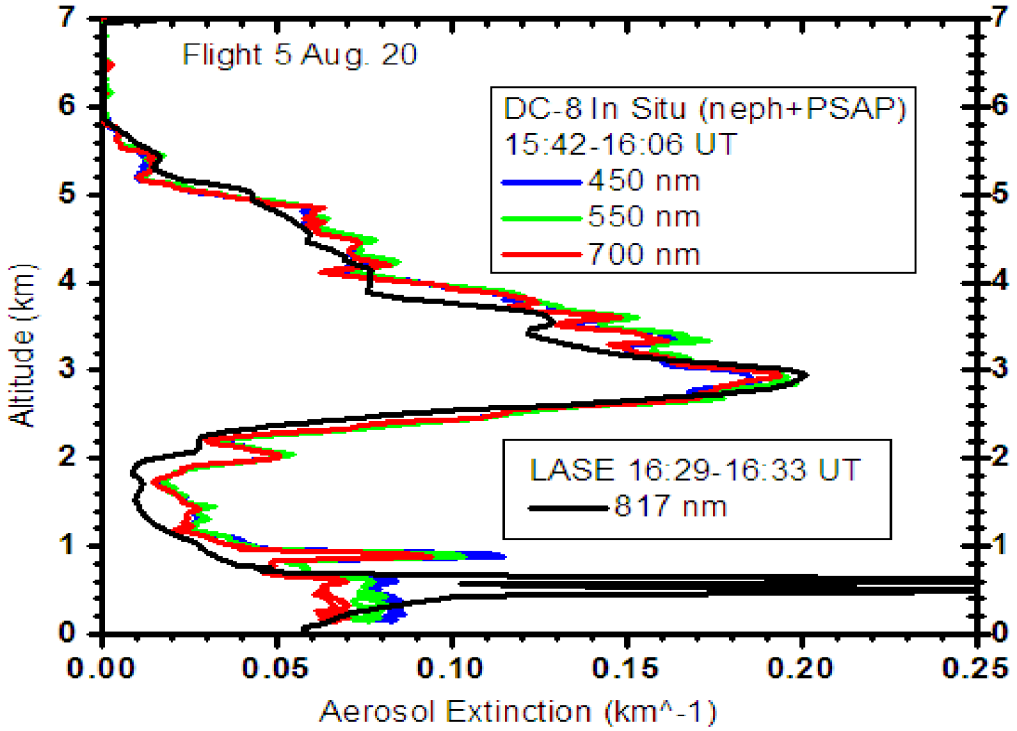

Fig. 8. Aerosol extinction profiles from LASE compared with *in situ* measurements from LARGE. The high scattering at 0.5 km seen in the LASE data are from a low altitude cloud.

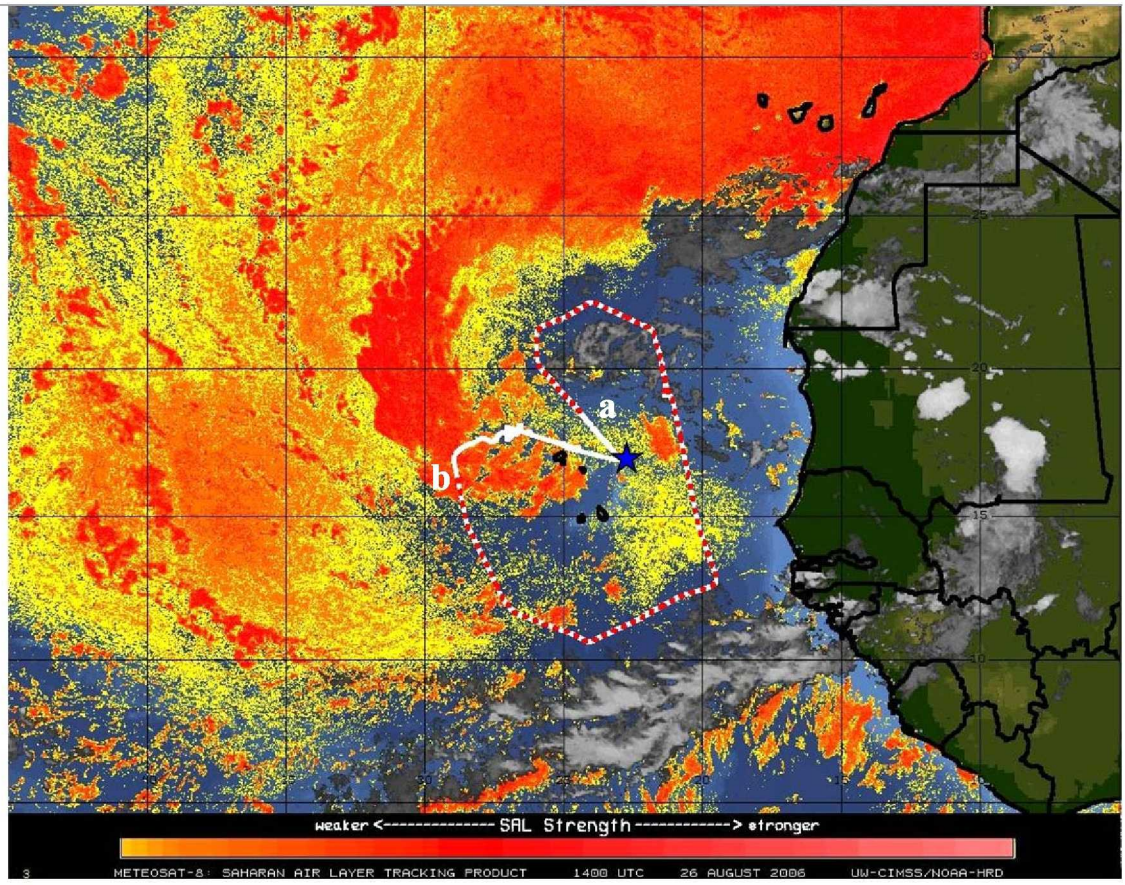

Fig. 9. METEOSAT-8 Split window image showing the distribution of the SAL on 26 Aug 2006. The DC-8 flight track is also shown and the segment of data shown in Fig. 10 is highlighted by red dash lines. The location of Sal Island, Cape Verde, Africa is indicated by the star symbol.

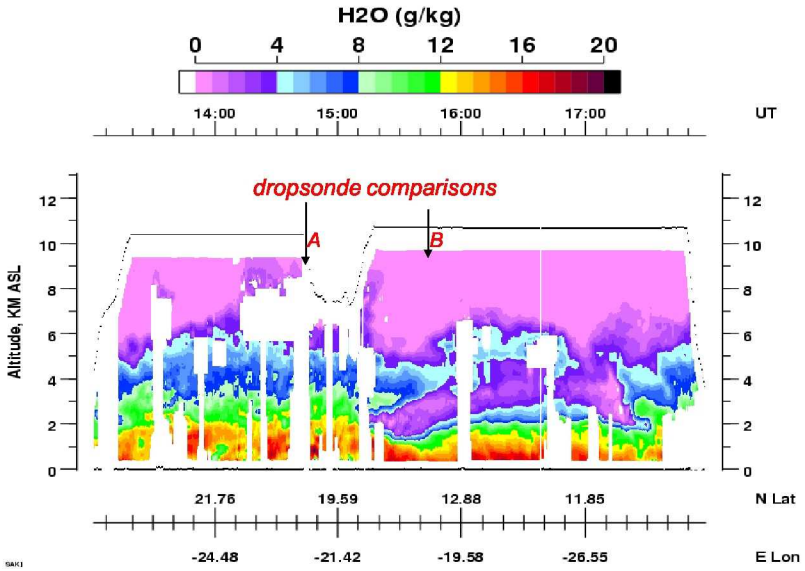

a)

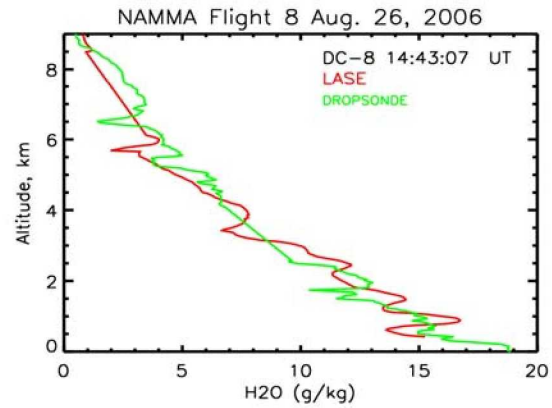

b)

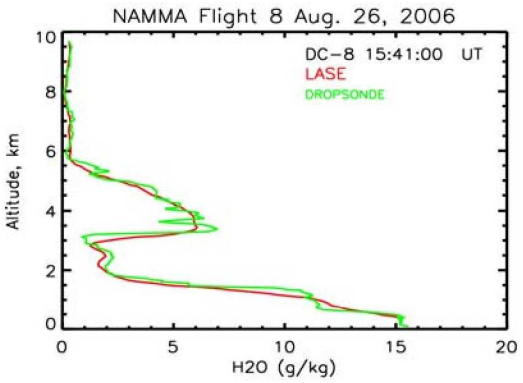

c)

Fig. 10. a) LASE measurements of water vapor mixing ratio distribution on 26 Aug. 2006 associated with an AEW and the surrounding dry air region, comparison of LASE water vapor mixing ratio with GPS dropsonde measurements identified at location b) A in Fig. 10a, and c) B in Fig. 10a.

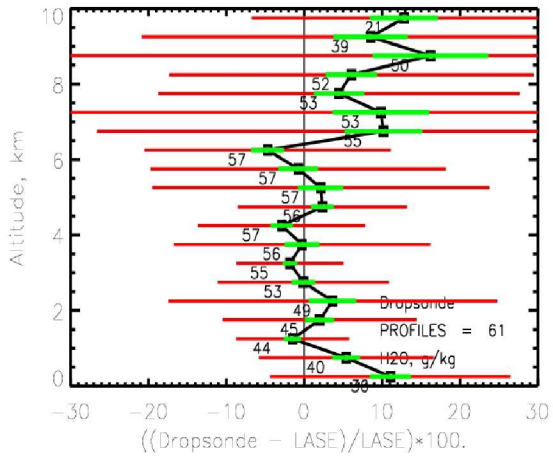

a)

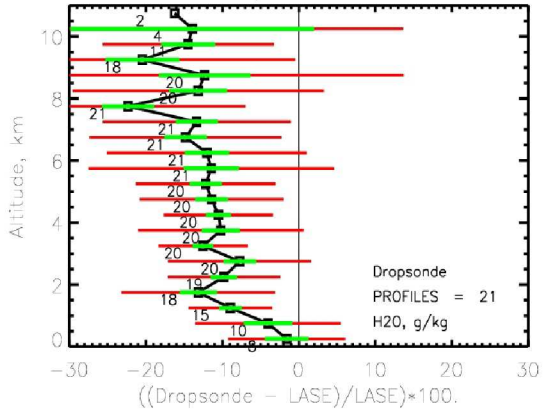

b)

Fig. 11. Comparison of LASE water vapor mixing ratio measurements a) new dropsondes and b) old dropsondes that were manufactured before 2001. The red error bars indicate the standard deviation of the differences and the green bars indicate the standard error.

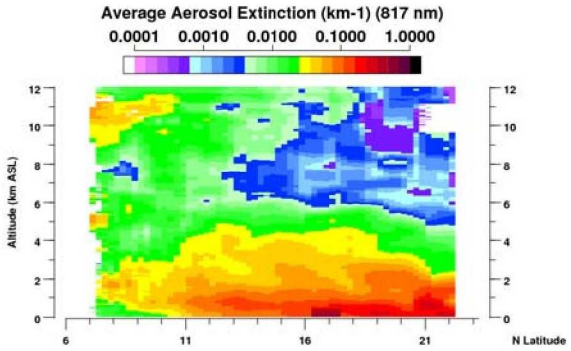
Average Aerosol Extinction (km-1) (817 nm)
0.0001 0.0010 0.0100 0.1000 1.0000
Altitude (km ASL)
N Latitude

a)

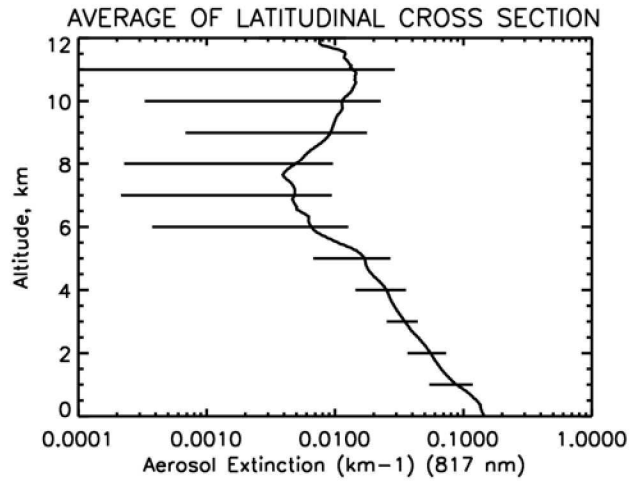
AVERAGE OF LATITUDINAL CROSS SECTION
Altitude, km
0.0001 0.0010 0.0100 0.1000 1.0000
Aerosol Extinction (km−1) (817 nm)

b)

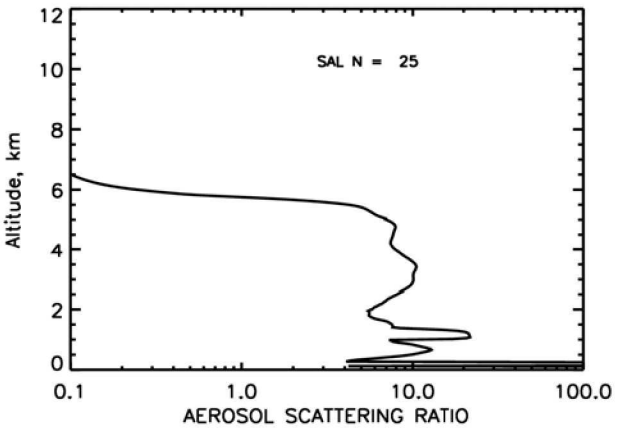
SAL N = 25
Altitude, km
0.1 1.0 10.0 100.0
AEROSOL SCATTERING RATIO

c)

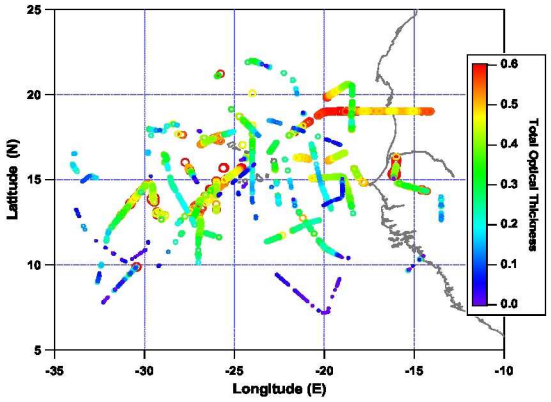

d)

Fig. 12. a) Latitudinal distribution of aerosol extinction profiles measured by LASE during NAMMA, b) average aerosol extinction profile from all observations and the error bars indicate the variability (standard deviation) c) average aerosol scattering ratio profile from clearly identified SAL regions and, d) the geographic distribution of the SAL optical thickness from NAMMA flights where the width of the symbols (circles) as well as the color scale indicate the optical thickness.

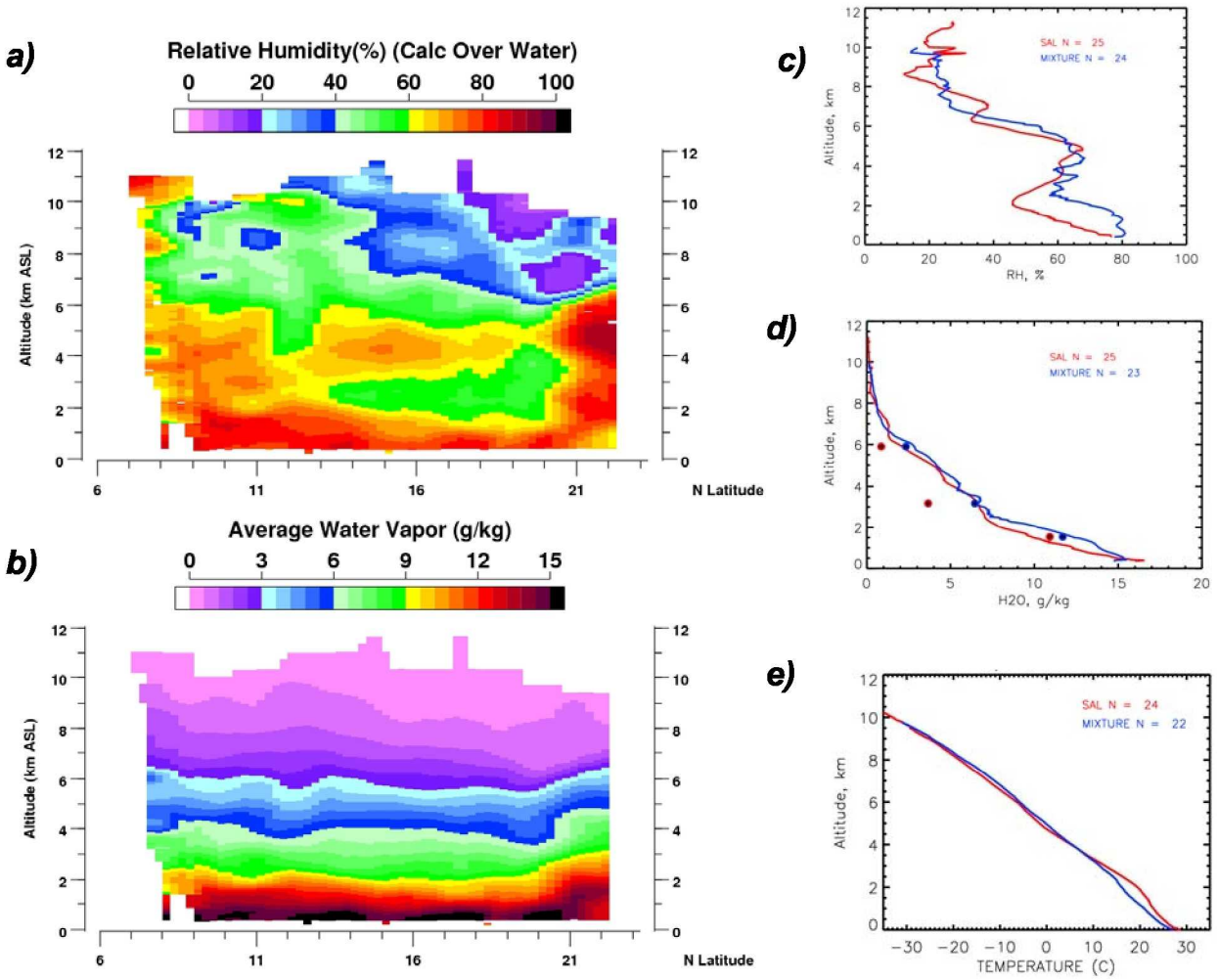

Fig. 13. a) Latitudinal distribution of RH distribution derived from LASE mixing ratio and dropsonde temperature profiles; b) latitudinal distribution of water vapor mixing ratios; c) average RH profile from all observations over the clearly identified SAL events and non-SAL (mixture) events; d) average water vapor mixing ratio profiles from SAL and non-SAL (mixture) events; and e) vertical profile of temperature from dropsondes from SAL and non-SAL events.